# Ultracompact Asymmetric Mach–Zehnder Interferometers with High Visibility Constructed from Exciton Polariton Waveguides of Organic Dye Nanofibers

*Ken Takazawa,* Jun-ichi Inoue, Kazutaka Mitsuishi, and Takashi Kuroda*

**Manipulation of light using subwavelength waveguides is a key technology in the development of miniaturized photonic circuits, which possess various advantages over their electronic counterparts. The novel approach presented for such waveguiding involves the propagation of exciton polaritons (EPs), which are quasi-particles formed by strong exciton–photon coupling, along organic dye nanofibers. A self-assembled nanofiber of thiacyanine (TC) with a width of ≈200 nm propagates the EPs created by an optical excitation over a submillimeter-scale distance and passes through a bend with a micrometer-scale radius with low bending loss. To demonstrate the remarkable potential of EP-based miniaturized photonic circuits, asymmetric Mach–Zehnder interferometers (AMZIs) are fabricated with TC nanofibers by micromanipulation. The AMZIs with a footprint of ≈20 μm × 20 μm exhibit a visibility of nearly unity and function as channel drop filters with the considerably high extinction ratio of up to ≈15 dB. Such high-performance and ultracompact channel drop filters operating in the visible wavelength region have rarely been developed with other waveguide technologies. The coherent properties of the EPs in the nanofibers are investigated using time-resolved experiments. The coherent properties provide useful information for designing EP-based photonic circuits and for understanding EP dynamics in a nanofiber.**

## 1. Introduction

Guiding and manipulating optical signals at the nano to micrometer scale are essential technologies for constructing miniaturized optical circuits, which have a number of important device applications in fields such as telecommunication, computing, and sensing.[1] Hence, subwavelength-scale waveguides based on photonic crystals,[2,3] structured metal surfaces,[4,5] semiconductor nanowires,[6,7] and silicon-on-insulator[8,9] have undergone extensive development to meet the requirement. Recently, we reported on a new approach for subwavelength waveguiding that uses the propagation of exciton polaritons (EPs) along organic dye nanofibers.[10] When a single crystalline nanofiber of thiacyanine dye (TC, **Figure 1**a) is excited by a focused laser beam with the energy of its exciton absorption band (≈2.6 eV), bright fluorescence spots are observed at both fiber tips, indicating that it functions as an efficient active waveguide (Figure 1b). Such active waveguiding has recently been observed in various organic nanofibers constructed from dyes and luminescent molecules.[11] We extensively investigated the active waveguiding in TC nanofibers and revealed that it is attributed to the propagation of the lower branch EPs formed by strong coupling between the excitons and the laser-induced fluorescence.[10]

EP waveguiding along nanofibers provides a striking advantage over light waveguiding along conventional waveguides in use for miniaturized photonic device applications. The EPs in a TC nanofiber can pass through a sharp bend of micrometer-scale radius ($r$) with low bending losses, enabling manipulation of the EPs on that scale.[12,13] This property is attributed to the large group index ($n_g$) of the nanofibers caused by the EP effect, namely, the strong exciton-photon coupling. The coupling leads to anti-crossing between dispersion curves of the exciton and the photon, and the resultant dispersion curves of EP exhibit two split branches, that is, the upper and lower EP branches.[14] The group velocity ($v_{EP}$) of the lower branch EPs is lowered with respect to that of the uncoupled light by the EP effect,[15,16] and as a result, $n_g$ (= $c/v_{EP}$) is elevated for the energy region of the lower EP branch. We experimentally determined the $n_g$ of TC nanofibers and found that it is indeed highly elevated to $n_g > 10$ near the exciton resonance.[10]

Here, we report on the fabrication of ultracompact asymmetric Mach–Zehnder interferometers (AMZI) using TC nanofibers by micromanipulation. The AMZIs are widely used photonic circuit components as channel drop filters, modulators, and switching devices.[17–19] In an AMZI, input light is split into two beams which are then recombined after traveling along paths of different lengths. Because of the phase difference between the two beams caused by the different path lengths, they interfere with each other, providing interference fringes in the output signal. To construct a miniaturized AMZI from optical waveguides, the waveguides must be bent at a small $r$ to create a path length difference. Thus, TC nanofibers are suitable building blocks

Dr. K. Takazawa, Dr. J. Inoue, Dr. K. Mitsuishi, Dr. T. Kuroda
National Institute for Materials Science
3-13 Sakura, Tsukuba 305-0003, Japan
E-mail: takazawa.ken@nims.go.jp

**DOI: 10.1002/adfm.201202108**

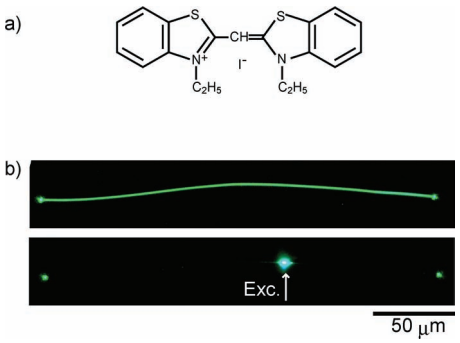


**Figure 1.** a) Chemical formula of thiacyanine (TC). b) Upper panel: fluorescence microscopy image of a TC nanofiber on a glass substrate. Excitation wavelength, $\lambda < 475$ nm; detection wavelength, $\lambda > 510$ nm. Lower panel: fluorescence microscopy image of the same nanofiber recorded by exciting it with a laser spot ($\lambda = 405$ nm) at the position labeled "Exc."

because of their capability to pass EPs through a sharp bend. Moreover, since an AMZI observes the interference between two EP beams, the coherent nature of EPs, which is derived from their light character, plays a key role in its operation. Therefore, an AMZI constructed from TC nanofibers effectively uses the half-matter half-light nature of EPs, and thus can clearly demonstrate the unique advantages of EP-based photonic devices. We show that our nanofiber AMZIs with a footprint of only ≈20 μm × 20 μm exhibited interference fringes with a visibility of nearly unity and functioned as high-performance channel drop filters for the visible wavelength region.

## 2. Results and Discussion

### 2.1. Nanofiber Geometry and Micromanipulation

TC nanofibers were synthesized via self-assembly in a solution.[20,21] The nanofibers have a rectangular cross section and a length of up to ≈250 μm. Width ($d$) of the nanofibers can be controlled from ≈100 nm to ≈1 μm by varying parameters in the synthesis (see Experimental Section). In our earlier study, we measured fluorescence microscopy images of single nanofibers with different $d$ by focused laser beam excitation and observed that those with $d <$ ≈400 nm did not exhibit the fluorescence spots at the fiber tips. On the basis of this observation, we deduced that $d >$ ≈400 nm is a necessary condition for a nanofiber to hold at least one propagation mode of the EPs.[20] However, in our recent studies, we found that detectability of the tip fluorescence strongly depends on the numerical aperture (NA) of the objective lens used for the microscopy. When we used an objective with NA = 0.95, we could clearly observe the tip fluorescence for fibers with $d \approx$ 200 nm, while we could not observe it with a NA = 0.5 objective. Thus, the EP propagation actually occurs even in narrow fibers with $d \approx$ 200 nm. The narrower the fibers, the more flexible they are. Flexibility is a beneficial property when constructing small devices by sharply bending the nanofibers. In this study, therefore, we

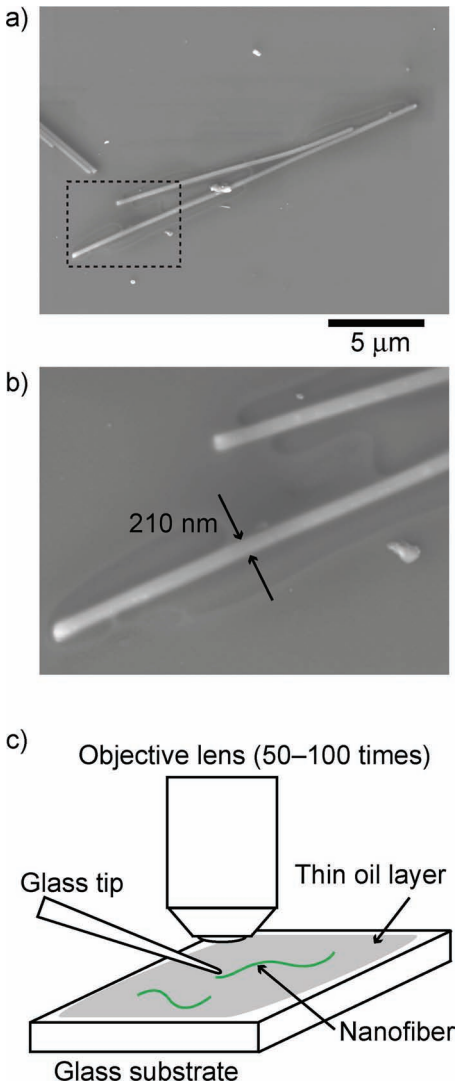


**Figure 2.** a) SEM image of nanofibers used for the AMZI fabrication. b) Magnified SEM image of the area surrounded by a dashed square in (a). Edges of a thin oil layer are visible around the nanofibers. c) Schematic illustration of micromanipulation of nanofibers.

used nanofibers with $d \approx$ 200 nm for the device fabrication. The strong NA dependence of the detectability of the tip fluorescence is probably related to the radiation angle of the fluorescence outcoupling from the fiber tips as well as its intensity; the narrow fibers may have a small radiation angle, which requires a high NA objective to collect the fluorescence from the direction normal to the fiber axis.

The nanofibers were dispersed on a glass substrate that was covered with a thin oil layer ($n \approx 1.48$) of a few tens of nanometers thickness. **Figure 2**a,b show scanning electron microscope (SEM) images of TC nanofibers with $d$ = 210 nm on the substrate, which were used to fabricate one of the AMZIs presented in this study (the nanofibers shown in **Figure 3**a). The nanofibers were manipulated by using a glass tip attached to a micromanipulator under microscope observations (Figure 2c).[13] The thin oil layer prevents the nanofibers from

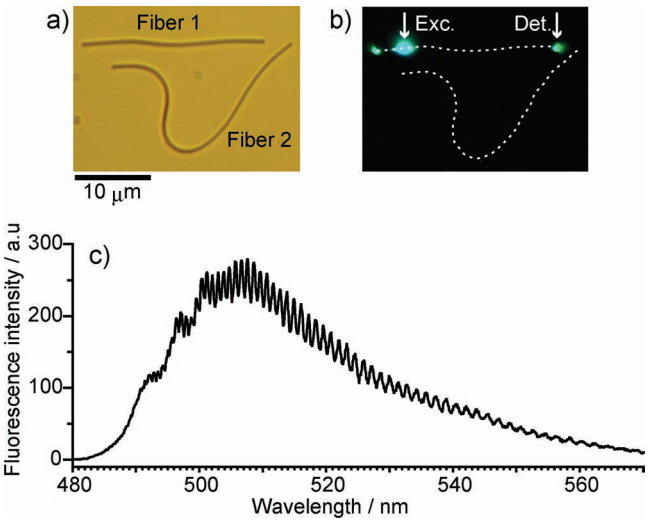


**Figure 3.** a) Optical microscopy image of nanofibers (Fibers 1 and 2), which were used for the AMZI fabrication. b) Fluorescence microscopy image of Fiber 1 recorded by exciting the position labeled "Exc." with a laser spot. Dashed lines representing Fibers 1 and 2 are eye guides. c) Spatially resolved fluorescence spectrum measured at the position labeled "Det." in (b).

adhering to the glass surface, thus significantly improving the manipulativeness of the nanofibers.

### 2.2. Fabrication and Characterization of AMZIs

Figure 3a shows an optical microscopy image of two nanofibers: Fiber 1 (length: 24.1 μm) and Fiber 2 (length: 39.3 μm). Width for both the nanofibers is $d$ = 210 nm. Before manipulating these nanofibers for the AMZI fabrication, we investigated the waveguiding property of Fiber 1, which was later used to evaluate the performance of the fabricated AMZI. The position near the right tip of Fiber 1 was excited with a diffraction limited laser spot ($\lambda$ = 405 nm, spot size: ≈300 nm) and the fluorescence spectrum at its left tip was recorded by spatially resolved fluorescence microscopy (Figure 3b).[12,13,21] The spectrum obtained shows a broad fluorescence ranging from ≈480 to ≈570 nm, which is ascribed to the propagation of the EPs from the excited position to the fiber tip (Figure 3c). A rapid oscillation of the fluorescence intensity with a period of 1–2 nm is attributed to the Fabry–Perot modes due to the reflection of the EPs at both the end faces of the nanofiber.[10,21]

We fabricated an AMZI by bending Fiber 2 and making both its end parts contact Fiber 1 (**Figure 4**a). In this device, EPs created near the left tip of Fiber 1 are split into two beams at the first junction through evanescent coupling. After traveling two paths with different lengths, they are recombined at the second junction. Then, the output signal is observed at the right tip of Fiber 1. The path length difference ($\Delta L$) of this device was 26.4 μm, and $r$ of the 180°-bend in Fiber 2 was ≈2.5 μm. Owing to the sharp bend, this device occupied an area of only ≈20 μm × 20 μm. To obtain the highest visibility in an AMZI, an input signal must be split into half at the first junction (3-dB coupler).

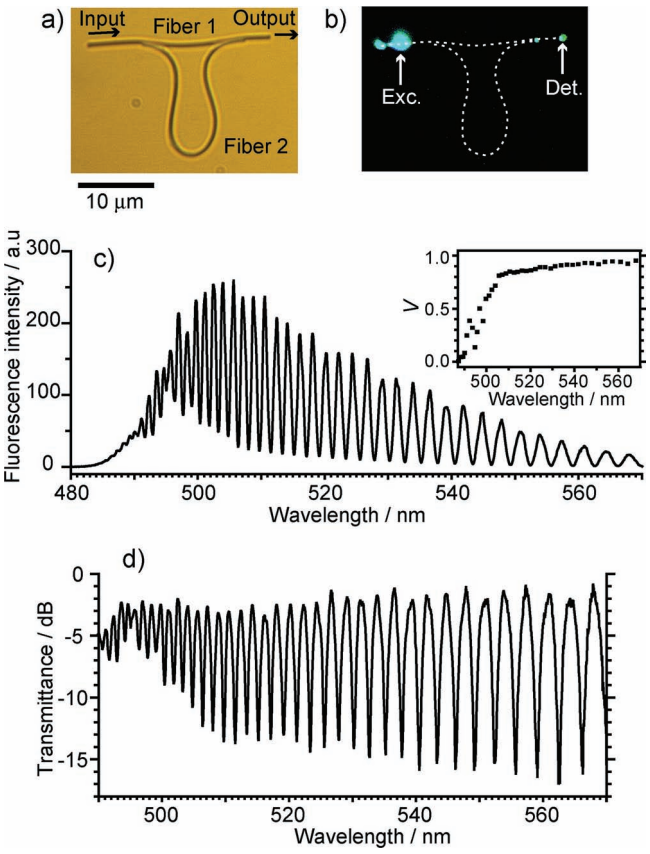


**Figure 4.** a) Optical microscopy image of the fabricated AMZI with $\Delta L$ = 26.4 μm. The contact length for both junctions is $l$ ≈ 1 μm. b) Fluorescence microscopy image of the AMZI recorded by exciting the position labeled "Exc." with a laser spot. Dashed lines representing the AMZI are guides for the eye. c) Spatially resolved fluorescence spectrum measured at the position labeled "Det." in (b). Inset: Plot of visibility $V$ as a function of $\lambda$. d) Transmittance spectrum of the AMZI.

In our nanofiber AMZI, the splitting ratio of the EPs at the junction can be tuned by adjusting the contact length between the two fibers ($l$). We first adjusted $l$ of both the junctions to ≈1 μm. We excited the position near the left tip of Fiber 1 to input the EPs to the device and recorded the fluorescence spectrum at the right tip of Fiber 1 (Figure 4b). The obtained output spectrum shows sharp interference fringes over its entire range (Figure 4c), proving that this device functioned as an AMZI. The visibility of the interference fringes is defined as

$$V = (I_{max} - I_{min})/(I_{max} + I_{min}), \quad (1)$$

where $I_{max}$ and $I_{min}$ are intensity maxima and minima in an interference fringe, respectively. $V$ was evaluated using Equation 1 and plotted in the inset of Figure 4c. $V$ was 0.8–1.0 for 510 nm < $\lambda$ < 570 nm, showing that almost perfect interference occurred in this wavelength region. For $\lambda$ < 510 nm, $V$ decreased with a decrease in $\lambda$, and the fringe vanished ($V$ = 0) at $\lambda$ ≈ 490 nm.

To evaluate the performance of this AMZI as a channel drop filter, we determined the transmittance of this device. The

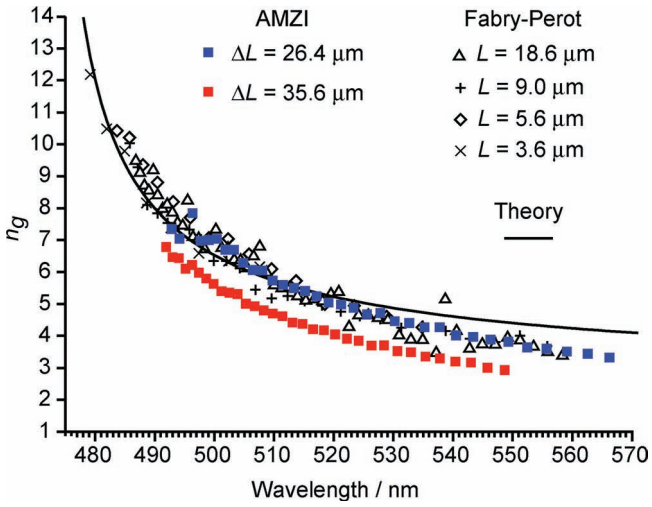


**Figure 5.** Plot of $n_g$ evaluated from the AMZIs with $\Delta L$ = 26.4 μm (blue squares) and with $\Delta L$ = 35.6 μm (red squares). Symbols show $n_g$ evaluated from the Fabry–Perot modes observed for nanofibers with different lengths ($L$ = 3.6–18.6 μm), and a solid curve shows $n_g$ obtained by the EP theory.[10]

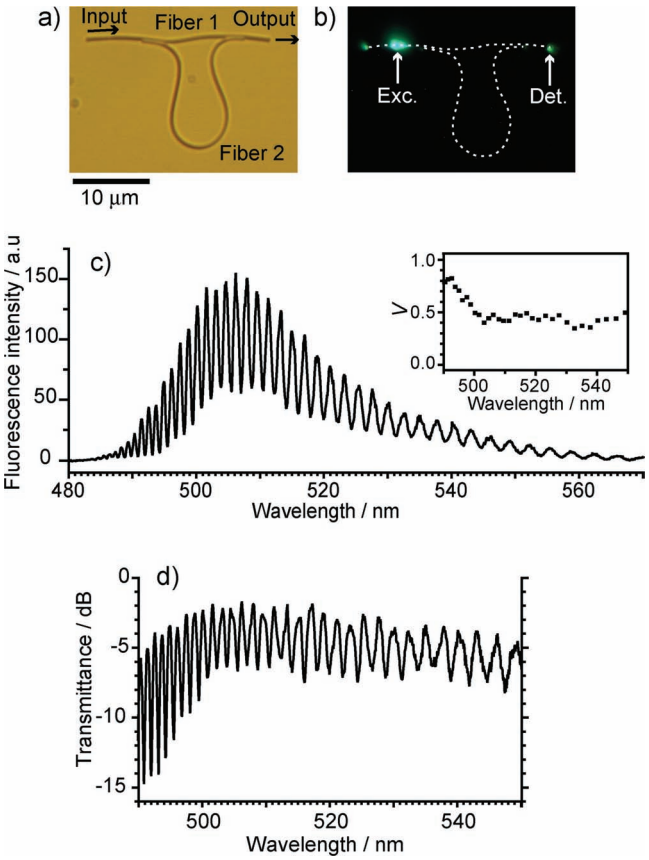


**Figure 6.** a) Optical microscopy image of the AMZI fabricated by modifying the junction parts of one shown in Figure 4. The contact length for both junctions is $l \approx 2$ μm. b) Fluorescence microscopy image of the AMZI recorded by exciting the position labeled "Exc." with a laser spot. Dashed lines representing the AMZI are eye guides. c) Spatially resolved fluorescence spectrum of the AMZI measured at the position labeled "Det." in (b). Inset: Plot of visibility $V$ as a function of λ. d) Transmittance spectrum of the AMZI.

output spectrum (Figure 4c) was normalized with respect to that of Fiber 1 measured before Fiber 2 was attached (Figure 3c). The obtained transmittance spectrum was plotted in decibels in Figure 4d. The extinction ratio defined as $r_e = T_{max}–T_{min}$ (= $10\log(I_{max}/I_{min})$) was 13–15 dB for 510 nm < λ < 570 nm, where $T_{max}$ and $T_{min}$ are transmittance maxima and minima, respectively. These $r_e$ values demonstrate a significantly high performance of this AMZI. For λ < 510 nm, $r_e$ decreased with a decrease in λ and dropped to 1–2 dB at λ ≈ 500 nm. The linewidths (3-dB widths, Δλ) of the drop channels were Δλ = 1.6 and 0.8 nm at λ = 560 and 510 nm, respectively, which showed a gradual decrease with a decrease in λ.

To confirm that these fringes are attributed to the interference of the EPs, we evaluated $n_g$ of the nanofibers from the observed fringe pattern. The value of $n_g$ is related to the spacing between fringes (free spectral range, $FSR$) through the following equation:

$$n_g = \lambda^2/(FSR \times \Delta L). \quad (2)$$

$FSR$ evaluated from the spectrum was $FSR$ = 3.3 nm at λ = 560, and decreased to $FSR$ = 1.3 nm at λ = 500 nm. The value of $n_g$ was calculated by using Equation 2 and plotted in **Figure 5** (blue squares) together with that obtained in our previous study.[10] They agree well with each other and show a divergent increase with a decrease in λ, which is a characteristic feature of $n_g$ for the lower branch EP.[10] These results confirm that the observed fringes are due to the interference of EPs. The interference order of an AMZI is given by $N = n_g\Delta L/\lambda$. By using the $n_g$ values, $N$ was calculated to $N \approx 170$ and 370 at λ = 560 and 500 nm, respectively.

The transmittance spectrum in Figure 4d shows that $r_e$ considerably decreased for λ < ≈510 nm. This suggests that the junctions of this AMZI did not function as the 3-dB couplers for the EPs in this wavelength region. As Figure 5 shows, $n_g$ dramatically increased with a decrease in λ. This implies that the EPs in the short wavelength region are strongly confined in a nanofiber. As a result, the transfer of half the EPs through the evanescent coupling requires longer $l$ than that for the weakly confined EPs in the long wavelength region. To achieve 3-dB coupling for λ < ≈510 nm, we modified the junctions of the AMZI. **Figure 6**a shows an optical microscopy image of the modified device, where $l$ was lengthened to ≈2 μm for both junctions. The output spectrum of this device was measured in the same manner as previously mentioned (Figure 6b). The spectrum again shows the sharp interference fringes, but its visibility was considerably changed by lengthening of $l$ (Figure 6c). $V$ was evaluated by using Equation 1 and plotted in the inset of Figure 6c. For λ < ≈510 nm, $V$ was increased from 0–0.5 to 0.5–0.8 by the modification, while $V$ was decreased from 0.8–1.0 to 0.4–0.5 for λ > 500 nm. The spectrum was then normalized, and the transmittance spectrum is displayed in Figure 6d. It can be seen that $r_e$ improved from 1–2 to 5–10 dB for λ < 500 nm, showing that the junctions nearly functioned as 3-dB couplers

for this wavelength region. Conversely, $r_e$ decreased from 13–15 to 3–5 dB for $\lambda > \approx 510$ nm. This decrease suggests that $l$ of ≈2 μm gave rise to over-transfer of EPs for $\lambda > 510$ nm; namely, more than half the EPs were transferred at the junctions. These results show that large $r_e$ of 10–15 dB can be obtained for the wide wavelength range of $\lambda = 490$–570 nm by adjusting $l$.

To obtain smaller *FSR* for increased channels, we attempted to fabricate an AMZI with a larger $\Delta L$. **Figure 7**a shows an optical microscopy image of an AMZI with $\Delta L$ = 35.6 μm, which was constructed from Fiber 1 (length: 14.2 μm) and Fiber 2 (length: 43.2 μm). Widths of both fibers are $d \approx$ 200 nm. The contact length of both junctions was adjusted to $l \approx 1$ μm. The elaborate manipulation of Fiber 2 allowed the device size to be maintained at ≈20 μm × 20 μm despite the large $\Delta L$. We excited near the left tip of Fiber 1 and recorded a fluorescence spectrum at the right tip of Fiber 1 (Figure 7b). The output spectrum shows the sharp interference fringes with narrower spacing compared with that of the previous AMZI, reflecting the longer $\Delta L$ (Figure 7c). *FSR* was evaluated to *FSR* = 2.4 and 1.2 nm at $\lambda$ = 540 and 500 nm, respectively. $V$ was then evaluated using Equation 1 and plotted in the inset of Figure 7c. For 510 nm < $\lambda$ < 540 nm, $V$ was 0.8–0.9 and decreased with a decrease in $\lambda$ for $\lambda$ < 510 nm. The value of $n_g$ was calculated using Equation 2 and plotted in Figure 5 (red squares). Although the obtained $n_g$ curve shows the divergent increase with a decrease in $\lambda$, as characteristic of the lower branch EP, the curve shifts downward by ≈1 with respect to those obtained from other data. We are not sure about the reason for this shift so far, but it may suggest that multiple bends with large bending angles can affect $n_g$ averaged over the path length. The interference order was calculated to $N \approx 230$ and 430 at $\lambda = 550$ nm and 500 nm, respectively. The transmittance spectrum was obtained in the same manner as previously described and is plotted in Figure 7d. For 510 nm < $\lambda$ < 540 nm, $r_e$ was 10–12 dB, again demonstrating the high performance of our AMZI. For $\lambda$ < 510 nm, $r_e$ showed a gradual decrease and dropped to ≈3 dB at $\lambda \approx 490$ nm. The value of $\Delta\lambda$ was 1.3 and 0.6 nm at $\lambda = 540$ and 500 nm, respectively. It showed a gradual decrease, similar to the previous devices.

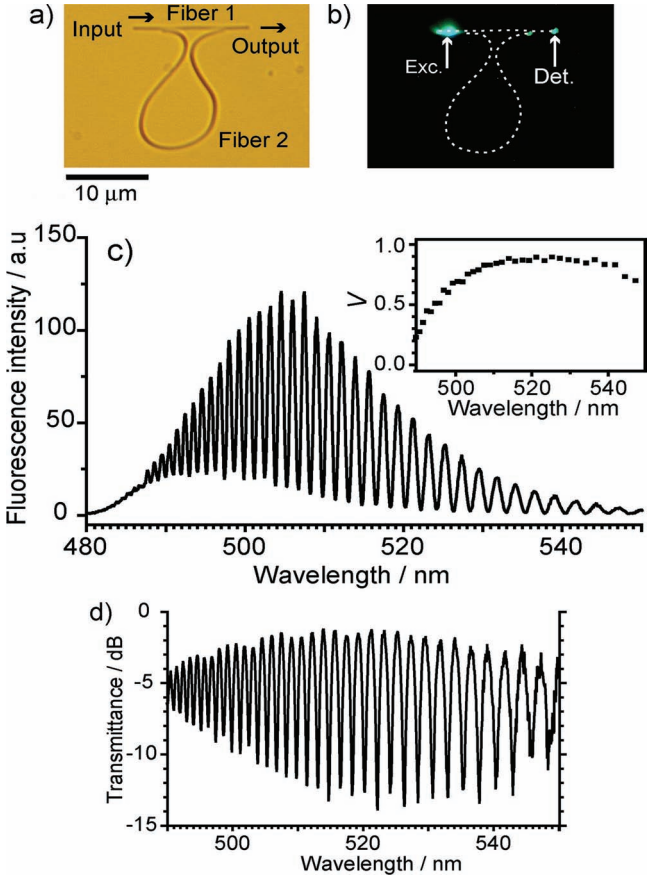


**Figure 7.** a) Optical microscopy image of the AMZI with $\Delta L$ = 35.6 μm. The contact length for both junctions is $l \approx 1$ μm. b) Fluorescence microscopy image of the AMZI recorded by exciting the position labeled "Exc." with a laser spot. Dashed lines representing the AMZI are eye guides. c) Spatially resolved fluorescence spectrum of the AMZI measured at the position labeled "Det." in (b). Inset: Plot of visibility $V$ as a function of $\lambda$. d) Transmittance spectrum of the device.

In addition to the compactness and the high-performance, a unique feature of our AMZIs, which may lead to even more advanced applications, is that they are constructed from nanofibers with strong optical activity. Recently, we reported that an irradiation of an electron beam to a TC nanofiber induces an irreversible decrease in its $n_g$.[22] It is of particular interest to examine the possibility of inducing a reversible $n_g$ change by utilizing the strong optical activity. It is well-known that the refractive index of optically active crystals can be reversibly changed by light irradiation through mechanisms such as inter- or intra-molecular structural changes by electronic excitation, thermo-optic effects, and photorefractive effects.[23,24] If we can reversibly change $n_g$ in one of the two arms of our AMZI by the light irradiation, it will be possible to control over the phase difference between the EP beams recombined at the junction. This allows the AMZIs to function as all-optical modulators and switching devices.[25,26] The development of such devices is a subject of our future research.

### 2.3. Coherent Properties of EPs in Nanofibers

In photonic circuits, a laser light, which has high temporal coherence, is commonly used as a signal light. Although in our nanofiber devices the nanofibers were excited by a laser beam, EPs are created not by coupling between the laser beam and the excitons, but by the coupling between the laser-induced fluorescence and the excitons. Thus, the coherent properties of EPs are largely governed by those of the fluorescence. Since the fluorescence generated by spontaneous emission is generally considered to be low coherent or incoherent light, EPs should likewise be low coherent. The low coherent nature may give rise to some restrictions in the photonic circuit application of nanofibers, especially if the circuits consist of such components as interferometers and resonators, in which coherence of a signal plays a crucial role. To clarify this point, below we investigate the coherent properties of EPs in TC nanofibers.

We can draw some information about the coherent properties from the results of the AMZIs presented above. The fact that our AMZIs exhibited high visibility implies that the two

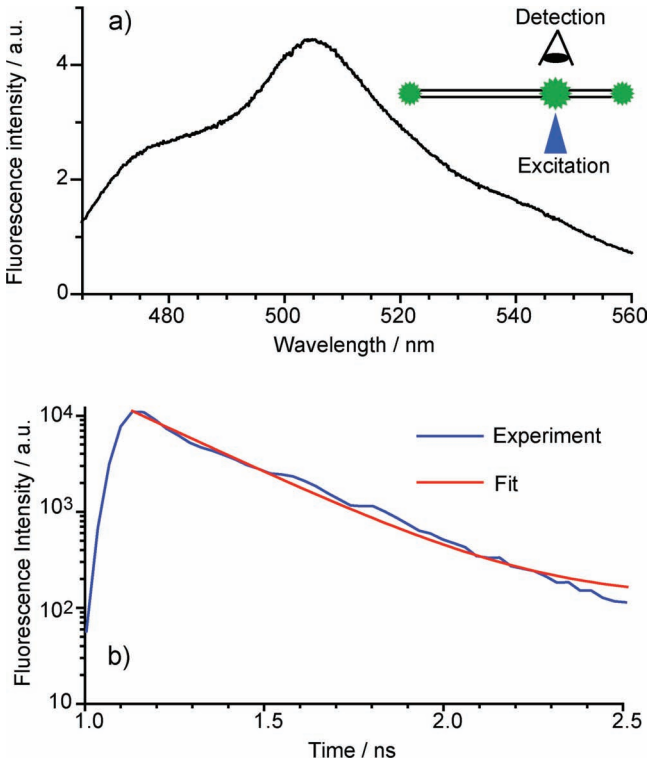


**Figure 8.** a) Spatially resolved fluorescence spectrum of a nanofiber recorded by exciting it with a laser spot and detecting the fluorescence from the position of the excitation. b) Fluorescence decay curve at $\lambda$ = 510 nm (blue curve) and best fitted curve (red curve).

EP beams recombined at the junction are coherent. For the two beams to be coherent, the coherence length ($l_c$) of the EPs must be longer than $\Delta L$, that is, $l_c > \Delta L$, and equivalently, the coherence time ($t_c = n_g l_c/c$) must be longer than $n_g \Delta L/c$, that is, $t_c > n_g \Delta L/c$. From the experimental observation that AMZI with $\Delta L$ = 35.6 µm exhibited the high visibility (Figure 7c), we can safely conclude that $l_c$ > 35.6 µm and $t_c > n_g \Delta L/c \approx 0.8$ ps ($n_g \approx 7$ at $\lambda$ = 500 nm). These $l_c$ and $t_c$ values are as short as those of light generally regarded as incoherent light. This means that an AMZI with a micrometer-scale $\Delta L$ does not require a highly coherent light source to exhibit high visibility.

As mentioned earlier, the EPs in a nanofiber are created by coupling between the fluorescence and the excitons. Thus, at the time when EPs are created, they should initially have $t_c$ equal to that of the fluorescence. The $t_c$ of fluorescence is equivalent to the fluorescence lifetime ($\tau_f$).[27] To evaluate $t_c$ of the EPs, therefore, we measured $\tau_f$ of a TC nanofiber. **Figure 8**a shows a spatially resolved fluorescence spectrum of a nanofiber recorded by exciting it with a laser spot and detecting the fluorescence at the excited position (see the inset in Figure 8a). We measured $\tau_f$ of the fluorescence at $\lambda$ = 510 nm by time-resolved fluorescence measurement. The fluorescence decay curve is shown in Figure 8b (blue curve). The curve was well fitted by a single exponential decay function (red curve), and $\tau_f$ was evaluated to $\tau_f = 248 \pm 6$ ps. This rather short $\tau_f$ values is typical for organic dye aggregates such as J- and H-aggregates.[28–32] The obtained lifetime leads to the conclusion that the EPs initially have $t_c$ = 248 ps and $l_c$ (= $t_c c/n_g$) ≈ 11 mm at $\lambda$ = 510 nm. Consequently, if we assume that the initial coherence is maintained during propagation, EPs are coherent over a 10-mm-scale distance along a nanofiber. Thus, as long as the path length of a device is within that scale, any restrictions that originate from the coherence properties of the EPs are not expected. However, the EPs should undergo decay of the coherence during propagation through a process such as scattering with phonons. This may reduce their coherence to a considerable extent. We will investigate the decay of the coherence, because it provides important information not only for designing nanofiber photonic circuits, but also for understanding EP dynamics in organic dye nanofibers.

## 3. Conclusions

By means of micromanipulation, we fabricated micrometer-sized AMZIs using self-assembled nanofibers of TC dye that propagate the EPs along the fibers. We revealed that EP propagation occurs in a nanofiber with subwavelength width of ≈200 nm. Owing to the high flexibility of the nanofibers and the elaborate micromanipulation, the fabricated AMZIs with $\Delta L$ = 26.4 and 35.6 µm occupied an area of only ≈20 µm × 20 µm. These AMZIs exhibited a visibility of nearly unity and functioned as channel drop filters with considerably high extinction ratios of up to ≈15 dB for the wavelength range of $\lambda$ = 490–570 nm. Such ultracompact, high-performance AMZI channel drop filters operating in the visible wavelength region have rarely been developed with other waveguide technologies. We suggested that potential applications of our AMZIs to all-optical modulators and switching devices utilizing the optical activity of the nanofibers. We further investigated the coherent properties of the EPs by fluorescence lifetime measurements. We revealed that the EPs initially have $t_c$ = 248 ps and $l_c$ = 11 mm at the time when they are created by laser excitation. These values imply that the EPs are coherent over a millimeter-scale distance along a nanofiber, if they maintain the initial coherence during propagation.

## 4. Experimental Section

*Sample Preparation*: TC was obtained from Hayashibara Corp. and used without further purification. TC in a ≈0.1 mM water solution at 40–80 °C self-assembled into nanofibers up to ≈250 µm long by cooling the solution to room temperature. The width of the nanofibers could be controlled from ≈100 nm to ≈1 µm by varying the solution temperature and/or cooling speed. A high solution temperature and high cooling speed led to the formation of narrower nanofibers. In the present study, a TC solution was prepared at 60 °C and cooled to room temperature at ambient conditions. This resulted in the formation of nanofibers whose width dispersed around 200 nm. A small amount of vacuum oil was deposited onto a glass substrate (microscope cover glass, 22 mm × 22 mm) and was repeatedly wiped with a lens cleaning paper to leave only a thin oil layer on the surface. The solution containing the nanofibers was drop-casted to the substrate and the solvent was allowed to evaporate.

*Electron Microscopy*: A scanning electron microscope (SEM, JEOL, JSM-6700F) was used. The sample was carbon coated to avoid charging. The low vapor pressure of the vacuum oil (<$1.3 \times 10^{-3}$ Pa) allowed the sample to be placed in an evacuated sample chamber of the SEM. SEM

measurement on the sample was performed after optical measurements on it were conducted.

*Micromanipulation*: A glass probe tip (diameter: ≈200 nm) attached to a piezo-micromanipulator (Kleindiek) was used for micromanipulation. The sample was placed on the motorized stage (Prior, H-101) of an optical microscope (Olympus, BX-51), and the nanofibers were manipulated by moving both the glass tip and the sample under microscope observation with a long-working-distance objective lens (50× or 100×).[13]

*Fluorescence Microscopy Imaging and Spatially Resolved Fluorescence Microscopy*: An output of a continuous wave diode laser (Coherent, Radius405, $\lambda$ = 405 nm) was coupled into an epi-illumination fluorescence microscope (Olympus, BX-51), and the laser beam was focused onto the sample with a 100× objective lens (NA = 0.95, spot size ≈ 300 nm). The fluorescence from the sample was collected by the same objective lens. In fluorescence microscopy imaging, the fluorescence was recorded by a color CCD camera (Jenoptic, ProgRes C10). In spatially resolved fluorescence microscopy, the fluorescence was imaged onto the entrance slits of an imaging monochromator (Acton Research, SpectraPro 2150). The fluorescence passing through the slits was recorded by a liquid-nitrogen-cooled back-illuminated CCD camera (Princeton Instruments, Spec10, 1340 × 400 pixels).

*Time-Resolved Fluorescence Measurements*: The second harmonic output ($\lambda$ = 400 nm) of a mode-locked Ti-sapphire laser (Coherent Mira 900, pulse width: 3 ps) operated at 3.8 MHz was focused on a nanofiber by a 50× objective lens (NA = 0.8). Fluorescence was collected by the same objective and detected by a microchannel plate photomultiplier tube (MCP-PMT, Hamamatsu, R3809U-51) through a spectrometer (Solar, MS2000). The output signal from the MCP-PMT was sent to a time-correlated single photon counter (Picoquant, PicoHarp 300), which measured photon arrival with a time resolution of ≈40 ps.

## Acknowledgements

The authors thank Drs. T. Takamasu and K. Sakoda for helpful discussions and Ms. Y. Nakayama for experimental assistance. This work was supported by the Grant-in-Aid for Scientific Research (No. 24540332), Japan Society for the Promotion of Science.

Received: July 26, 2012
Published online: September 24, 2012

[1] R. G. Hunsperger, *Integrated Optics: Theory and Technology*. 5th ed., Springer, Berlin, Germany **2002**.
[2] A. Mekis, J. C. Chen, I. Kurland, S. H. Fan, P. R. Villeneuve, J. D. Joannopoulos, *Phys. Rev. Lett.* **1996**, *77*, 3787.
[3] S. Noda, K. Tomoda, N. Yamamoto, A. Chutinan, *Science* **2000**, *289*, 604.
[4] S. A. Maier, P. G. Kik, H. A. Atwater, E. Harel, B. E. Koel, A. A. G. Requicha, *Nat. Mater.* **2003**, *2*, 229.
[5] S. I. Bozhevolnyi, V. S. Volkov, E. Devaux, J. Y. Laluet, T. W. Ebbesen, *Nature* **2006**, *440*, 508.
[6] C. J. Barrelet, A. B. Greytak, C. M. Lieber, *Nano Lett.* **2004**, *4*, 1981.
[7] M. Law, D. J. Sirbuly, J. C. Johnson, J. Goldberger, R. J. Saykally, P. D. Yang, *Science* **2004**, *305*, 1269.
[8] M. Lipson, *J. Lightwave Technol.* **2005**, *23*, 4222.
[9] B. Jalali, S. Fathpour, *J. Lightwave Technol.* **2006**, *24*, 4600.
[10] K. Takazawa, J. Inoue, K. Mitsuishi, T. Takamasu, *Phys. Rev. Lett.* **2010**, *105*, 067401.
[11] a) Y. S. Zhao, H. B. Fu, A. D. Peng, Y. Ma, D. B. Xiao, J. N. Yao, *Adv. Mater.* **2008**, *20*, 2859; b) Y. S. Zhao, A. D. Peng, H. B. Fu, Y. Ma, J. N. Yao, *Adv. Mater.* **2008**, *20*, 1661; c) Y. S. Zhao, H. B. Fu, A. D. Peng, Y. Ma, Q. Liao, J. N. Yao, *Acc. Chem. Res.* **2010**, *43*, 409; d) F. S. Kim, G. Q. Ren, S. A. Jenekhe, *Chem. Mater.* **2011**, *23*, 682; e) Y. S. Zhao, J. J. Xu, A. D. Peng, H. B. Fu, Y. Ma, L. Jiang, J. N. Yao, *Angew. Chem. Int. Ed.* **2008**, *47*, 7301; f) M. Schiek, F. Balzer, K. Al-Shamery, J. R. Brewer, A. Lutzen, H.-G. Rubahn, *Small* **2008**, *4*, 176; g) Q. L. Bao, B. M. Goh, B. Yan, T. Yu, Z. A. Shen, K. P. Loh, *Adv. Mater.* **2010**, *22*, 3661; h) C. Zhang, C. L. Zou, Y. L. Yan, R. Hao, F. W. Sun, Z. F. Han, Y. S. Zhao, J. N. Yao, *J. Am. Chem. Soc.* **2011**, *133*, 7276; i) C. Zhang, Y. S. Zhao, J. N. Yao, *Phys. Chem. Chem. Phys.* **2011**, *13*, 9060; j) Q. H. Cui, Y. S. Zhao, J. N. Yao, *J. Mater. Chem.* **2012**, *22*, 4136; k) F. Balzer, V. G. Bordo, A. C. Simonsen, H. G. Rubahn, *Appl. Phys. Lett.* **2003**, *82*, 10; l) F. Balzer, V. G. Bordo, A. C. Simonsen, H. G. Rubahn, *Phys. Rev. B* **2003**, *67*, 115408.
[12] K. Takazawa, *Chem. Phys. Lett.* **2008**, *452*, 168.
[13] K. Takazawa, J. Inoue, K. Mitsuishi, T. Takamasu, *Adv. Mater.* **2011**, *23*, 3659.
[14] J. J. Hopfield, *Phys. Rev.* **1958**, *112*, 1555.
[15] R. G. Ulbrich, G. W. Fehrenbach, *Phys. Rev. Lett.* **1979**, *43*, 963.
[16] S. Chu, S. Wong, *Phys. Rev. Lett.* **1982**, *48*, 738.
[17] W. E. Martin, *Appl. Phys. Lett.* **1975**, *26*, 562.
[18] R. A. Becker, *Appl. Phys. Lett.* **1983**, *43*, 131.
[19] C. C. Teng, *Appl. Phys. Lett.* **1992**, *60*, 1538.
[20] K. Takazawa, Y. Kitahama, Y. Kimura, G. Kido, *Nano Lett.* **2005**, *5*, 1293.
[21] K. Takazawa, *J. Phys. Chem. C* **2007**, *111*, 8671.
[22] K. Takazawa, K. Mitsuishi, J. Inoue, *Appl. Phys. Lett.* **2011**, *99*, 253302.
[23] *Photorefractive Effects and Materials*, (Eds: P. Gunter, J. P. Huignard), Springer-Verlag, New York **1988**.
[24] Y. Zhang, T. Wada, H. Sasabe, *J. Mater. Chem.* **1998**, *8*, 809.
[25] K. Tajima, *Jpn. J. Appl. Phys.* **1993**, *32*, 1746.
[26] G. Assanto, G. Stegeman, M. Sheikbahae, E. Van Stryland, *Appl. Phys. Lett.* **1993**, *62*, 1323.
[27] R. Loudon, *The Qunatum Theory of Light*, 1st ed., Oxford University Press, Oxford **1973**.
[28] *J-aggregates*, (Ed: T. Kobayashi), World Scientific Publishing, Singapore **1996**.
[29] D. Möbius, *Adv. Mater.* **1995**, *7*, 437.
[30] F. Fink, E. Klose, K. Teuchner, S. Dähne, *Chem. Phys. Lett.* **1977**, *45*, 548.
[31] H. Yao, S. Sugiyama, R. Kawabata, H. Ikeda, O Matsuoka, S. Yamamoto, N. Kitamura, *J. Phys. Chem. B* **1999**, *103*, 4452.
[32] R. F. Khairutdinov, N. Serpone, *J. Phys. Chem. B* **1997**, *101*, 2602.